Time-Resolved Fluorescent Imaging of Glucose

Michael Schäferling,[1,2] Meng Wu,[1] and Otto S. Wolfbeis[1]

A method for the fluorescent imaging of glucose is described that is based on the detection of enzymatically produced hydrogen peroxide, using the europium(III) tetracycline complex as the fluorescent probe incorporated into a hydrophilic polymer layer. Coadsorption of glucose oxidase (GOx) makes these sensor layers respond to the hydrogen peroxide produced by the GOx-assisted oxidation of glucose. The hydrogel layers are integrated into a 96-microwell plate for a parallel and simultaneous detection of various samples. Glucose is visualized by means of time resolved luminescence lifetime imaging. Unlike in previous methods, the determination of H_2O_2 does not require the addition of peroxidase or a catalyst to form a fluorescent product. The lifetime-based images obtained are compared with conventional fluorescence intensity-based methods with respect to sensitivity and the dynamic range of the sensor layer. The main advantages provided by this sensing scheme for H_2O_2 include reversibility, applicability at neutral pH, and the straightforwardness of the transducer system and the imaging device.

KEY WORDS: Optical sensor; time-resolved fluorescence imaging; europium tetracycline; glucose sensor.

INTRODUCTION

Glucose is ubiquitous in living nature and plays an essential role in all processes related to life. It is by far the most important direct source of energy in cells and the building block for numerous other saccharides. Not surprisingly, its determination in all kinds of matrices including blood and other body fluids is one of the most often performed assays. While a seemingly uncounted number of assays has been reported for glucose, it was only in the past 15 years that methods for continuous monitoring of glucose have become available [1], mainly with the aim to develop sensors that are needed in context with the design of an artificial pancreas. For sensing devices electrochemical [2–7], fluorescence-based [8–10] and nearinfrared [11] methods are predominant besides the commercial colorimetric test strips. It is interesting to note, though, that practically all methods for determination of glucose are based on either sampling at a discrete sampling site (such as the artery), or on continuous sensing at a single site. Imaging, in contrast, allows the concentration of a species to be "seen" in a fairly large area. Imaging, therefore, yields an information that otherwise is available with a whole array of single sensors only.

Imaging of oxygen, for example, turned out to be particularly useful since oxygen sensor membranes (which are easily prepared) can be deposited on almost any subject of interest including the inner wall of bioreactor vessels [12], on the bottom of microtiterplates (MTPs) [13], in (and on) transplanted organs, on skin [14], to give informations related to general physiology, in studies on cellular system and aggregates, and during the monitoring the growth of artificial organs including chondrocytes [12].
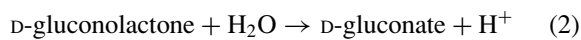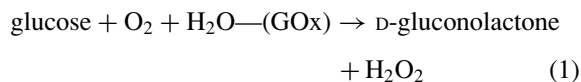
Among the optical methods for imaging, fluorescence is a particularly promising kind of spectroscopy for application in spatially-resolved detection of chemical species. One may differentiate between three techniques of fluorescence imaging. The first consists in imaging the natural fluorescence of the species of interest, for example NADH or FAD [15–19]. The second consists in the

[1] Institute of Analytical Chemistry, Chemo- and Biosensors, University of Regensburg, 93040 Regensburg, Germany.
[2] To whom correspondence should be addresssed. E-mail: michael. schaeferling@chemie.uni-regensburg.de

specific ("immunohistochemical") fluorescent labeling of the species of interest by exposing the area of interest to a fluorescently labeled antibody that binds to the species of interest. This method is limited, though, to immunogenic species, and not applicable to glucose. Fluorescence in-situ hybridization, in turn, is applicable to nucleic acids only [20–23]. A third method consists in a combination of sensor technology with fluorescence imaging technology. Here, the region of interest is covered with a few μm thick fluorescent sensor layer that undergoes a change in its fluorescence properties if equilibrated with the species to be imaged. Typical examples include sensors for oxygen, temperature, pH, and the like [13,24–27]. The first and third method are applicable to in-vivo studies.

Despite numerous attempts, there is no fluorescent probe available at present that would enable the direct probing of glucose at near neutral pH. Thus, indirect methods were developed. They are based on the detection of one of the species produced in the GOx-assisted oxidation of glucose, followed by hydrolysis:

$$glucose + O_2 + H_2O—(GOx) \rightarrow \text{D-gluconolactone}$$
$$+ H_2O_2 \quad (1)$$
$$\text{D-gluconolactone} + H_2O \rightarrow \text{D-gluconate} + H^+ \quad (2)$$

For example, fluorescent sensor membranes have been described that are based on the measurement of the consumption of oxygen during GOx-catalyzed oxidation of glucose [28,29]. This approach, while working well in clinical assays, suffers from the variable oxygenation of the sample, thus requiring the oxygen level to be measured in a second assay. Other schemes have been reported where the decrease in pH is measured, but this approach suffers from the varying buffer capacity of the system to be investigated.

Since glucose and dextran bind reversibly to concanavalin A (Con A), a smart sensing approach has been developed by *Schultz et al.* [30] that relies on the competitive binding of fluorescently labeled dextran and glucose for the binding site of Con A which is immobilized on sepharose. The fiber optic sensor only "sees" the unbound dextran whose concentration is high in presence of excess glucose. The scheme can be extended to fluorescence energy transfer [31]. A similar approach has been described by *Lakowicz* [32], who has also applied anthracene derivatives for a lifetime-based sensing of glucose [33]. Another fluorescent detection scheme is based on the conformational changes of the galactose/glucose-binding protein (GPB) upon binding to glucose [34]. However, all these methods cannot be applied to imaging.

The ideal species to be detected in GOx-based asays is based on the measurement of the hydrogen peroxide (H_2O_2) produced according to Eq. (1). H_2O_2 is not present in most samples and thus does not form an unknown background. We have recently introduced [35] a new fluorescent probe for H_2O_2 that responds to it by an up to 15-fold increase in fluorescence intensity and a change in the average decay time from 30 to 60 μs. Europium (III) tetracycline [Eu(Tc)] is applicable at near-neutral pHs and—unlike other probes for H_2O_2—does not require the presence of a peroxidase. [Eu(Tc)] can be immobilized on hydrophilic sensor membranes [36,37] of a typical thickness of 1–5 μm and these can be deposited on the subject of interest. Thus, such sensors membranes (which are easily prepared) are ideally suited for sensing and imaging of glucose via the H_2O_2 produced by its GOx-assisted oxidation.

MATERIALS AND METHODS

Chemicals and Reagents

Tetracycline hydrochloride was from Serva (Heidelberg, Germany; www.serva.de), europium chloride from Alfa Products (Danvers, MA; www.alfa.com). The MOPS buffer was obtained by dissolving 691 mg of 3-(N-morpholino)propanesulfonic acid (3.3 mmol) and 370 mg of sodium 3-(N-morpholino)-propanesulfonate in water, and adjusting the pH to 6.9 with minute quantities of hydrochloric acid. The reagent solution of the [Eu(Tc)] complex was obtained by dissolving 4.8 mg of EuCl$_3$ · 6 H$_2$O (130 μmol) and 2.0 mg of tetracycline hydrochloride (41.5 μmol) in 200 mL of the MOPS buffer. The Hypan hydrogel (HN80) was from Hymedix (Dayton, NJ; see: www.hymedix.com).

Preparation of Sensor Membranes

In order to cast a sensor membrane, a cocktail was prepared by dissolving 2.5 g of the hydrogel in 47.5 g of dimethylsulfoxide (DMSO). The mixture was stirred for 20 h at 80°C after which a clear, slightly yellow and viscous cocktail was obtained. This mixture was spread on a dust-free, dry and optically transparent ethyleneglycol-terephthalate polyester support (Mylar™, prod. no. LS 146585; from Goodfellow Cambridge, Huntington, UK; www.goodfellow.com) using a knife-coating device with a spacer distance of 120 μm. This layer was first air-dried for 1 hr. After extensive washing with distilled water, the membrane was stored in water for 2 hr, taken out, and cut into circular spots. A typical sensor spot is 1.0–2.5 cm in diameter.

A solution was prepared containing 4 mg of glucose oxidase (GOx, type VII-S; 50 000 units/g, from Sigma) in 80 μL of MOPS buffer of pH 6.9. The GOx solution was dropped onto the sensor spot and evenly distributed. After incubation on air for 12 hr the enzyme was immobilized on the sensor film by physical adsorption. The sensor layer was stored in MOPS buffer for 24 hr and then in [Eu(Tc)] reagent solution (see above) for 4 hr. After taking out it was rinsed with copious quantities of distilled water. Finally, it was stored at 4°C in buffer containing 0.01% sodium azide as a biocide.

Preparation of Sensor Arrays

The preparation of the microwell plate sensor format was conducted in two ways. In the first, 5 μL of the polymer cocktail (5% in DMSO) were deposited in the single wells of a microtiterplate. After drying, the fluorescent probe was immobilized in the polymer layer by adding subsequently 50 μL of the GOx solution and 50 μL of the [Eu(Tc)] reagent solution to every well, as described above. In the second method, the rear panel of a black polystyrene 96-microwell plate (Greiner Bio-One, Frickenhausen, Germany; www.greinerbioone.com) was removed, and the sensor membrane fixed on the back of the plate with the help of black silicone rubber.

Spectra and Instrumentation

Fluorescence spectra were recorded using an Aminco-Bowman Series 2 luminescence spectrometer (SLM-Aminco, Rochester, NY) equipped with a continuous wave 150-W xenon lamp as a light source. Fluorescence was excited at 405 nm and emission collected at 616 nm. The bandpasses were set to 16 nm both in excitation and emission. All experiments were performed at room temperature in a flow cell with an inner volume of ca. 300 μL. The beam of the exciting light was directed onto the sensor membrane in the center of the flow cell through a plexiglass wall at an angle of ca. 50°, and emitted (fluorescent) light was collected by the lens of the detection path of the fluorometer and directed onto the photomultiplier tube via the monochromator system and after passing a 580-nm longpass filter.

Luminescence intensities on the 96-microwell plates were recorded with a Tecan GENios Plus microplate reader at an excitation wavelength of 405 nm and an emission wavelength of 612 nm in presence of different glucose concentrations.

Imaging Device

The set-up of the imaging system consists of a fast gateable CCD-camera (SensiMod from PCO GmbH, Kelheim, Germany; see: www.pco.de), a pulsable LED array with 96 UV light emitting diodes ($\lambda_{max} = 405$ nm, Roithner Laser Technik, Vienna; see: www.roithner-laser.com), a pulse generator (Scientific Instruments DG 535), optical excitation (BG 12; Schott) and emission filters (KV 550; Schott) and a personal computer for controlling and visualization of the experiments. The self-developed software modules have been described previously [13,24]. For a typical imaging experiment, the rear panel of a black polystyrene 96-microwell plate (Greiner) was removed, and a sensor membrane fixed on the back of the plate with black silicon rubber. Eight adjacent wells were then spotted with solutions containing glucose in varying concentrations. Images were taken after a 10 min incubation time and evaluated with a second image processing software module (IDL, Research Systems, Inc., Boulder, CO; www.rsinc.com).

RESULTS AND DISCUSSION

Spectral Properties of the Sensor Membrane

The probe [Eu(Tc)] undergoes an up to 15-fold increase in luminescence intensity at an emission wavelength of 616 nm after excitation with a 405-nm diode laser on exposure to hydrogen peroxide. The increase can also be observed for the side emission bands at 577 and 592 nm, respectively. Simultaneously, large changes in the luminescence decay time can be observed. It is assumed that [Eu(Tc)] can reversibly bind H_2O_2 which thereby replaces water molecules ligated to the europium cation, to form the more strongly fluorescent [Eu(Tc)(H_2O_2)] complex. This behavior can be exploited for the determination of glucose by simple addition of GOx and [Eu(Tc)] to a sample at pH ~7 [35].

In order to obtain a sensor membrane, the [Eu(Tc)] complex was immobilized in a hydrophilic polymer matrix. It consists of a copolymer composed of polyacrylonitrile ("hard") and polyacrylamide ("soft") blocks. The less hydrophilic polyacrylonitrile domains are responsible for the retaining of organic molecules or metal-ligand probes such as [Eu(Tc)]. Hypan hydrogels are insoluble in water and most organic solvents except dimethylsulfoxide, and exhibit excellent permeability for ions and hydrophilic species including glucose. The increase in fluorescence intensity of the sensor membrane after exposure to different glucose concentrations is shown in Fig. 1.
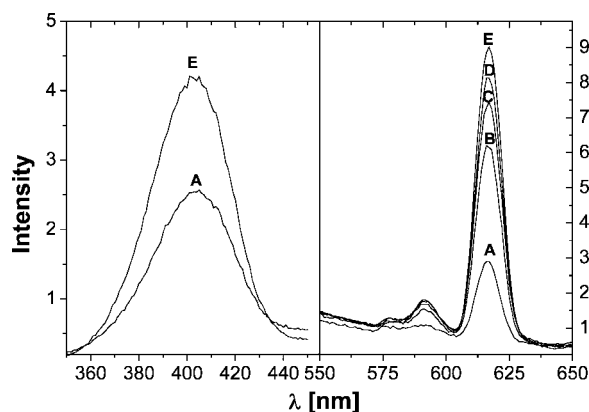
Fig. 1. Excitation spectra (left, emission wavelength 616 nm) and emission spectra (right, excitation wavelength 405 nm) of the [Eu(Tc)]/GOx sensor membrane recorded in a flow cell in presence of different glucose concentrations in MOPS buffer after 20 min exposure time at pH 6.9. $A = 0, B = 1, C = 2, D = 4, E = 8$ mmol L^{-1} glucose.
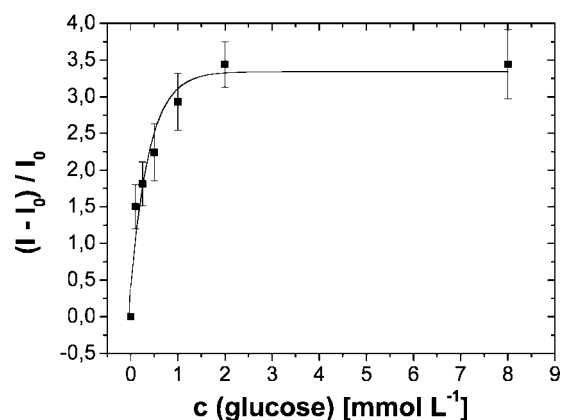

Fig. 2. Calibration plot $[(I - I_0)/I_0]$ versus the glucose concentration in MOPS buffer (pH 6.9). I_0 is the initial time-gated fluorescence intensity of the sensor membrane in absence of glucose, and I the intensity in presence of glucose. The error bars demonstrate the standard deviations calculated from 8 identical spots.

The fluorescence decay characteristics of [Eu(Tc)] is rather complex and strongly depends on the additional ligation of H_2O_2. Thus, the main component of [Eu(Tc)] has an average decay time of $\sim$30 μs which is shifted to $\sim$60 μs in case of [Eu(Tc) (H_2O_2)] [37]. As a result, the time-resolved ("gated") fluorescence detection of H_2O_2 via [Eu(Tc)] is best performed after a time lag of at least 30 μs.

Time-Gated Luminescence Intensity Measurements

The long fluorescence lifetime of the [Eu(Tc)] complex and the special decay characteristics offer the opportunity for timegated measurements for the quantification of fluorescence intensities. For this purpose, the sensor membranes were incorporated into a polypropylene 96-microwell plate and first analyzed by a time-resolving microplate fluorescence reader in presence of 9 different concentrations of glucose. Each concentration was measured on 8 different spots. The highest sensitivities (in terms of signal increase) were obtained by measuring at a time lag of 40 μs after the LEDs were switched off,

with a signal integration time of 100 μs. A further advantage of this time-gated method is due to the fact that the background fluorescence of the plate material and of biological species in the sample (both with ns lifetimes) have decayed after the 40 μs time lag. Table I shows the relative fluorescence intensities as a function of the glucose concentration, averaged over 8 spots.

The fluorescence intensity of the sensor membrane increases by a factor of 4.5 on exposure to a 2 mmol L^{-1} glucose solution. The dynamic range of the time-gated detection scheme covers glucose concentrations from below 0.1 to 2 mmol L^{-1}. The intensity remains nearly constant at concentrations of >2mmol L^{-1}, indicating that the sensor becomes saturated. The standard deviations are rather high ($\sim$10%) and indicate the presence of inhomogeneities between the single spots which is not unusual for intensity-based measurements. Figure 2 shows a normalized calibration plot $[(I - I_0)/I_0]$ in the concentration range between 0 and 8 mmol L^{-1} of glucose, representing the dynamic range of the sensor. The linear range of this glucose sensor method extends from 0 to 0.5 mmol L^{-1}. The limit of detection (LOD, defined as $3 \times$ SD/slope of linear range) is around 0.05 mmol L^{-1} glucose.

Table I. Effect of the Glucose Concentration on the Averaged Time-Resolved Fluorescence Intensity I of [Eu(Tc)]/GOx Sensor Spots Incorporated into a Microwell Plate, and Respective Standard Deviations (SD) Calculated from 8 Spots

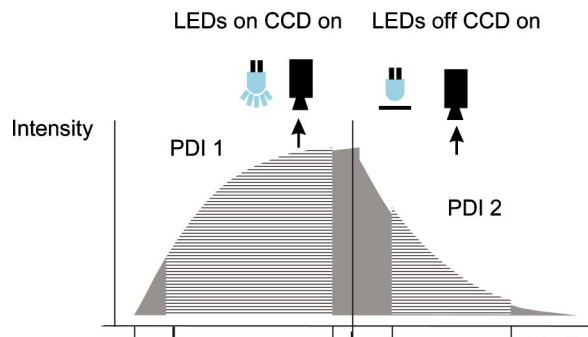| | c (Glucose) [mmol L^{-1}] | | | | | | | | | | | |
	0	0.1	0.25	0.5	1	2	4	8	12	Blank	Blank + EuTc	Blank + GOx
I	6267	15659	17651	20201	24662	27799	26542	27795	26684	39	9917	36
SD%	9.7	9.5	10.6	12.0	9.9	7.0	9.4	10.5	16.5			

Fig. 3. Schematic representation of the time gates applied in the phase delay ratioing (PDR) imaging mode. Image PDI 1 is obtained during excitation of the probe [Eu(Tc)] between 30 and 80 μs; image PDI 2 is taken in the decay phase in a time window between 130 and 190 μs.

Table II. Effect of the Glucose Concentration on the Ratiometric Imaging R Values of the Fluorescent Sensor Foil (See Eq. (1) and Fig. 4), and Standard Deviations (SD) in the Center of the Sensor Spots

	c (Glucose) [mmol L^{-1}]							
	0	0.005	0.01	0.05	0.1	0.2	0.5	1
R_{PDR}	8.17	7.49	7.15	6.24	5.59	4.86	3.70	3.61
SD%	1.6	0.5	0.9	0.6	0.2	0.4	0.3	0.9

Ratiometric Fluorescence Lifetime Imaging of the Sensor Membrane Array

For the application in imaging experiments, the polymeric sensor foil was fixed on the back of a black microwell plate as described in the experimental section. Time-resolved imaging of fluorescence intensities were performed in the *phase delay ratioing* (PDR) mode [38,39]. Excitation was accomplished by using a 96-array of violet LEDs having a peak output at 405 nm, which exactly matches the absorption peak of [Eu(Tc)]. The imaging set-up, consisting of an LED array, optical filters, and a CCD camera [13], as well as the whole data acquisition process [24], have been demonstrated recently in detail. The microwell plate was covered with a light-guiding adapter, consisting of 96 optical fibers ($\varnothing = 2$ mm), which reduces the imaged area to a size that matches the focus of the CCD camera.

In the PDR mode, the sensor spots are first excited by a short pulse of light (duration from $t = 0$–90 μs, see Fig. 3) and the luminescence intensity was acquired over

two time gates to give two images. Phase delay image no. 1 (refered to as PDI 1) was taken during the excitation period (LED on, with a time window t_1 between 30 and 80 μs). Phase delay image no. 2 (PDI 2) was acquired in the emission period (LED off, time window t_2 from 130 to 190 μs). Figure 4 illustrates this time-gated ratiometric process. Both images were corrected for their respective background dark images, recorded in a second measurement cycle. The data acquisiton software finally calculated the two intensity distributions and visualized the intrinsically referenced ratio according to

$$R_{PDR} = (PDI\,1)/(PDI\,2) \qquad (3)$$

In a typical imaging experiment, 8 adjacent wells of the microwell plate equipped with the sensor membrane were spotted with different concentrated glucose solutions in MOPS buffer (Fig. 5). The glucose concentration range was adjusted to between 0 and 4 mmol L^{-1} (see the data in Table II). Then the fluorescence images of the microwell plate were recorded by the imaging device and processed with the help of the IDL software module.

The visualization and quantitative evaluation of the images reveals an excellent homogeneity of the fluorescence intensitiy ratios in the center of the single spots, indicated by the low standard deviations of below 1% in
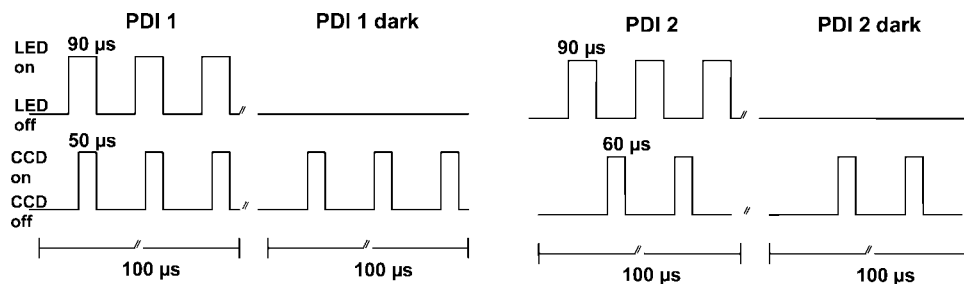

Fig. 4. Time course of the data acquisition process. The images for the different gates (PDI 1, PDI 1 dark, PDI 2, PDI 2 dark) are acquired one after the other and summed and averaged separately. After subtraction of the background dark pictures, the ratio R_{PDR} is calculated according to Eq. (3).
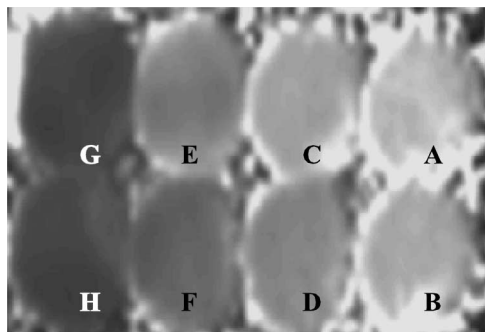
Fig. 5. Grey-scale ratiometric fluorescence image of sensor membrane spots in a microwell plate exposed to different glucose concentrations in MOPS buffer. $A = 0$, $B = 0.005$, $C = 0.01$, $D = 0.05$, $E = 0.1$, $F = 0.25$, $G = 0.5$, $H = 1$ mmol L^{-1} glucose.

the center regions. The intensity ratios R_{PDR} decrease from approximately 8.2 to 3.6 on going from glucose concentrations of 0 to 1 mmol L^{-1}. The dynamic range of the ratiometric imaging covers concentrations from 0.005 to 1 mmol L^{-1} of glucose. At higher concentrations the intensity signals become saturated. Figure 6 shows the normalized calibration plot $[(R_0 - R)/R_0]$ for the time-resolved ratiometric measurement in the dynamic concentration range.

As a result, the linear range of this ratiometric imaging sensor is between 0 to 0.05 mmol L^{-1} glucose. The calculated limit of detection (LOD) amounts to 0.003 mmol L^{-1} glucose. Alternatively, the ratiometric fluorescence signal distribution on the sensor array can be visualized and quantified directly by a three-dimensional plot with the intensity ratio R as Z-axis. Figure 7 shows an example
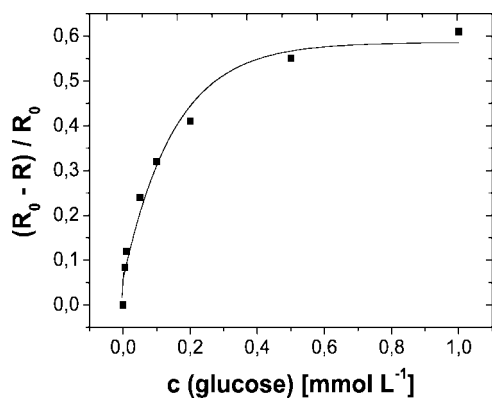

Fig. 6. Calibration plot $[(R_0 - R)/R_0]$ versus the concentration of glucose in MOPS buffer at pH 6.9. R_0 is the initial ratiometric fluorescence intensity of the sensor membrane, and R the intensity in presence of increasing concentrations of glucose.
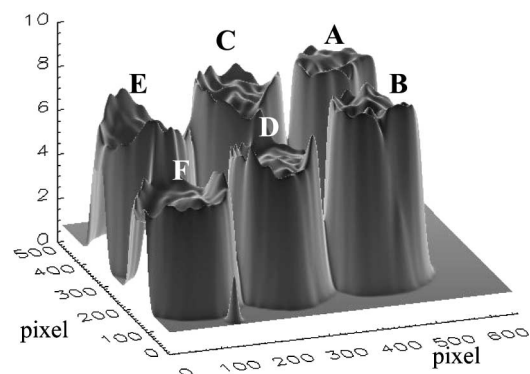

Fig. 7. Time-resolved ratiometric image of the glucose sensor spots in a microwell plate format visualized as a 3D plot. The spots represent different glucose concentrations in the single wells. $A = 0$, $B = 0.005$, $C = 0.01$, $D = 0.05$, $E = 0.1$, $F = 0.25$ mmol L^{-1} glucose.

of such a 3D illustration for the linear range of the sensor array.

Ratiometric Lifetime Imaging in Solution

In order to compare the performance of the imaging scheme of the immobilized sensor with the probe in solution, ratiometric images were also acquired of the [Eu(Tc)] probe in solution. The grey-scale image shown in Fig. 8 demonstrates the enhancement of the ratiometric fluorescence emission of the [Eu(Tc)] probe in solution spotted on a microwell plate, in presence of glucose and GOx.

For further quantitative measurements, 200 μL of a solution of [Eu(Tc)] ($c = 100$ μmol L^{-1}) and glucose oxidase (12 U mL^{-1}) in MOPS buffer (10 mM, pH 6.9) were placed in the single wells of a microplate and exposed for 20 min to glucose concentrations between 1.4 and 700 μmol L^{-1}. Figure 8 shows the corresponding image of the plate for 10 different glucose concentrations (1–12), each concentration spotted three times (see Table III).
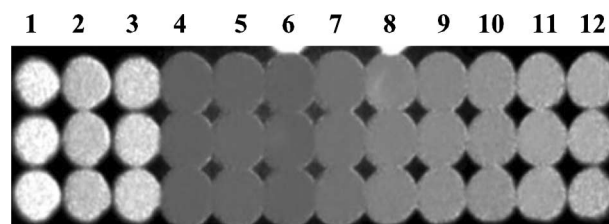

Fig. 8. Grey-scale ratiometric fluorescence image of the [Eu(Tc)]/GOx glucose assay in solution, spotted on a microwell plate and exposed to different glucose concentrations in MOPS buffer. For concentrations see Table III.

Table III. Effect of the Glucose Concentration on the Ratiometric Imaging R Values (See Fig. 7) on the [Eu(Tc)]/GOx Fluorescent Probe in Solution, and Standard Deviations (SD) Calculated from Three Identical Spots

	c (Glucose) [μmol L^{-1}]											
	0[a]	0[b]	28 [c]	700	280	140	70	28	14	7	2.8	1.4
Spot column	**1**	**2**	**3**	**4**	**5**	**6**	**7**	**8**	**9**	**10**	**11**	**12**
R_{PDR}	7.94	6.26	6.79	3.66	3.77	3.69	4.13	4.58	4.81	5.03	5.49	5.77
SD%	2.4	1.1	0.7	0.1	1.1	1.1	0.7	0.4	1.9	0.4	0.2	1.2

[a] [Eu(Tc)] blank.

[b] [Eu(Tc)] + GOx blank.

[c] [Eu(Tc)] + glucose blank (without GOx); c [Eu(Tc)]= 100 μmol L^{-1}; GOx = 12 U mL^{-1}.

The calibration plot (Fig. 9) shows that the system can image glucose concentrations in a dynamic range from around 1 to 150 μmol L^{-1}. The linear range of this assay extends from 0 to 15 μmol L^{-1}. The calculated limit of detection (LOD) is 0.5 μmol L^{-1}. The low standard deviations around 1%, calculated from three spots with equal concentrations, and the good homogeneity inside the microwells demonstrate the high reproducibility of ratiometric imaging methods. The detection limit for the [Eu(Tc)]/GOx assay in solution is almost six times lower than that of the sensor membrane. Thus, immobilization of both the europium complex and glucose oxidase in the polymer matrix is at the expense of sensitivity. On the other hand, the sensor membranes show a much broader dynamic range (see Fig. 7).

Besides of their high sensitivity, the presented sensing schemes offer additional unique properties, including (a) physiological pH conditions (b) a very large Stokes shift (210 nm), which helps to eliminate background signals from the light source with simple optical broadband edge filters, (c) an absorption maximum of 405 nm that exactly matches the line of the 405 nm-diode laser and of violet LEDs, and (d) a decay time in the μs range that permits the suppression of the fast decaying background fluorescence caused by the polymer layer, the microwell plate, and other fluorescent species in complex biological samples.

CONCLUSION

We introduce the first scheme for imaging glucose, one of the most important energy sources in biological organisms. Fluorescent sensor membranes were prepared that contain the hydrogen peroxide-sensitive probe [Eu(Tc)] and the enzyme glucose oxidase. No additional enzymes like peroxidases or catalase are required. While the glucose-sensitive membranes were arranged in a microwell plate format, it is conceivable that the sensor membranes may be arranged in numerous other ways to meet the particular needs of specific applications (e.g. for monitoring/imaging glucose in bioreactors, growing artificial tissue or cellular aggregates). We demonstrate that the ratiometric lifetime imaging provides a detection limit for the sensor of 0.003 mmol L^{-1} glucose which is more than ten times less than time-gated intensity measurements performed with commercially available microplate fluorescence readers, and nearly two magnitudes lower than fluorescence intensity measurements without time resolution. The ratiometric method also enables an intrinsic referencing of the intensity signals, which leads to a better homogeneity within the sensor spots and a higher reproducibility of the results compared to imaging methods based on signal intensity.
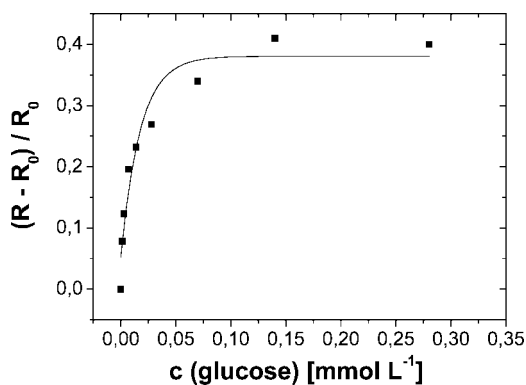

Fig. 9. Plot of [$(R_0$-$R)/R_0$] versus the concentration of glucose in MOPS buffer. R_0 is the initial ratiometric fluorescence intensity of the [Eu(Tc)]/GOx assay in solution, and R the intensity in presence of increasing concentrations of glucose.

REFERENCES

1. E. A. Hall (1990). *Biosensors*, Open University Press, Buckingham, pp. 253–282.

2. K. Habermüller, A. Ramanavicius, V. Laurinavicius, and W. Schuhmann (2000). An oxygen-insensitive reagentless glucose biosensor based on osmium-complex modified polypyrrole. *Electroanalysis* **12**, 1383–1389.

3. D. B. Papkovsky (1995). New oxygen sensors and their application to biosensing. *Sens. Actuat. B* **29**, 213–218.

4. J. Kulys (1999). The carbon paste electrode encrusted with a microreactor as glucose biosensor. *Biosens. Bioelectron.* **14**, 473–479.

5. A. Poscia, M. Mascini, D. Moscone, M. Luzzana, G. Caramenti, P. Cremonesi, F. Valgimigli, C. Bongiovanni, and M. Varalli (2003). A microdialysis technique for continuous subcutaneous glucose monitoring in diabetic patients. *Biosens. Bioelectron.* **18**, 891–898.

6. F. Ricci, C. Goncalves, A. Amine, L. Gorton, G. Palleschi, and D. Moscone (2003). Electroanalytical study of prussian blue modified glassy carbon paste electrodes. *Electroanalysis* **15**, 1204–1211.

7. S. F. White, A. P. F. Turner, U. Biltewski, J. Bradley, and R. D. Schmid (1995). On-line monitoring of glucose, glutamate and glutamine during mammalian cell cultivations. *Biosens. Bioelectron.* **10**, 543–551.

8. R. Narayanaswamy and F. Sevilla (1988). *Anal. Lett.* **21**, 1165–1175.

9. B. P. H. Schaffar and O. S. Wolfbeis (1990). A fast responding fibre optic glucose biosensor based on an oxygen optrode. *Biosens. Bioelectron.* **5**, 137–148.

10. O. S. Wolfbeis, I. Oehme, N. Papkovskaya, and I. Klimant (2000). Sol–gel based glucose biosensors employing optical oxygen transducers, and a method for compensating for variable oxygen background. *Biosens. Bioelectron.* **15**, 69–76.

11. H. M. Heise (2000) in R. A. Meyers (Ed.), *Encyclopedia of Analytical Chemistry*, Wiley, New York, pp. 56–83.

12. K. Kellner, G. Liebsch, I. Klimant, O. S. Wolfbeis, T. Blunk, M. B. Schulz, and A. Göpferich (2002). Determination of oxygen gradients in engineered tissue using a fluorescent sensor. *Biotechnol. Bioeng.* **80**, 73–83.

13. G. Liebsch, I. Klimant, B. Frank, G. Holst, and O. S. Wolfbeis (2000). Luminescence lifetime imaging of oxygen, pH, and carbon dioxide distribztion using optical sensors. *Appl. Spectrosc.* **54**, 548–559.

14. P. Babilas, V. Schacht, G. Liebsch, O. S. Wolfbeis, M. Landthaler, M. Szeimies, and C. Abels (2003). Effect of light fractionation and different fluence rates on photodynamic therapy with 5′-aminolaevulinic acid in vivo. *Br. J. Cancer* **88**, 1462–1469.

15. A. Shiino, M. Haida, and B. Beauvoit, and B. Chance (1999). Three-dimensional redox image of the normal gerbil brain. *Neuroscience* **91**, 1581–1585.

16. R. E. Anderson and F. B. Meyer (2002). In C. K. Sen and L. Packer (Eds.), *Methods in Enzymology*, Vol. 352, Academic Press, San Diego, pp. 482–494.

17. M. Hashimoto, Y. Takeda, T. Sato, H. Kawahara, O. Nagano, and M. Hirakawa (2000). Dynamic changes of NADH fluorescence images and NADH content during spreading depression in the cerebral cortex of gerbils. *Brain Res.* **872**, 294–300.

18. A. V. Kuznetsov, O. Mayboroda, D. Kunz, K. Winkler, W. Schubert, and W. S. Kunz (1998). Functional imaging of mitochondria in saponin-permeabilized mice muscle fibers. *J. Cell Biol.* **140**, 1091–1099.

19. M. Weinlich and H. Acker (1990). Flavoprotein-fluorescence imaging for metabolic studies in multicellular spheroids by means of confocal scanning laser microscopy. *J. Microsc.* **160**, RP1–RP2.

20. S. Van Stedum and W. King (2002). Basic FISH techniques and troubleshooting. *Methods Mol. Biol.* **204**, 51–63.

21. T. Liehr and U. Claussen (2002). Multicolor-FISH approaches for the characterization of human chromosomes in clinical genetics and tumor cytogenetics. *Curr. Genom.* **3**, 213–235.

22. B. Rautenstrauss and T. Liehr (2002). *FISH Technology*, Springer-Verlag, Berlin, Germany, 494 pp.

23. M. Andreeff and D. Pinkel (1999). *Introduction to Fluorescence In Situ Hybridization: Principles and Clinical Applications*, Wiley-Liss, New York, 455 pp.

24. G. Liebsch, I. Klimant, C. Krause, and O. S. Wolfbeis (2001). Fluorescent imaging of pH with optical sensors using time domain dual lifetime referencing. *Anal. Chem.* **73**, 4354–4363.

25. G. Liebsch, I. Klimant, and O. S. Wolfbeis, (1999). Cross-reactive metal ion sensor array in a micro titer plate format. *Adv. Mat.* **11**, 1296–1299.

26. K. M. Hanson, M. J. Behne, N. P. Barry, T. M. Mauro, E. Gratton, and R. M. Clegg (2002). Two-photon fluorescence lifetime imaging of the skin stratum corneum pH gradient. *Biophys. J.* **83**, 1682–1690.

27. P. C. Schneider and R. M. Clegg (1997). Rapid acquisition, analysis, and display of fluorescence lifetime-resolved images for real-time applications. *Rev. Sci. Instr.* **68**, 4107–4119.

28. M. C. Moreno-Bondi, O. S. Wolfbeis, M. J. P. Leiner, and B. P. H. Schaffar (1990). Oxygen optrode for use in a fiber-optic glucose biosensor. *Anal. Chem.* **62**, 2377–2380.

29. O. S. Wolfbeis, I. Oehme, N. Papkovskaya, and I. Klimant (2000). Sol—gel based glucose biosensors employing optical oxygen transducers, and a method for compensating for variable oxygen background. *Biosens. Bioelectron.* **15**, 69–76.

30. J. S. Schultz, S. Mansouri, and I. J. Goldstein (1982). Affinity sensor: A new technique for developing implantable sensors for glucose and other metabolites. *Diabetes Care* **5**, 245–254.

31. D. Meadows and J. S. Schultz (1988). Fiber-optic biosensors based on fluorescence energy transfer. *Talanta* **35**, 145–153.

32. L. Tolosa, H. Szmacinski, G. Rao, and J. R. Lakowicz (1997). Lifetime-based sensing of glucose using energy transfer with a long lifetime donor. *Anal. Biochem.* **250**, 102–108.

33. N. DiCesare and J. R. Lakowicz (2001). Evaluation of two synthetic glucose probes for fluorescence-lifetime-based sensing. *Anal. Biochem.* **294**, 154–160.

34. L. L. E. Salins, R. A. Ware, C. M. Ensor, and S. Daunert (2001). A novel reagentless sensing system for measuring glucose based on the galactose/glucose-binding protein. *Anal. Biochem.* **294**, 19–26.

35. O. S. Wolfbeis, A. Dürkop, M. Wu, and Z. Lin, (2002). A europium-ion-based luminescent sensing probe for hydrogen peroxide. *Angew. Chem.* **114**, 4681–4684; *Angew. Chem. Int. Ed.* **41**, 4495–4498.

36. O. S. Wolfbeis, M. Schäferling, and A. Dürkop, (2003). Reversible optical sensor membrane for hydrogen peroxide using an immobilized fluorescent probe, and its application to a glucose biosensor. *Microchim. Acta* **143**, 221–227 .

37. M. Schäferling, M. Wu, J. Enderlein, H. Bauer, and O. S. Wolfbeis (2003). Time-resolved luminescence imaging of hydrogen peroxide using sensor membranes in a microwell format. *Appl. Spectrosc.* **57**, 1386–1392.

38. P. Hartmann and W. Ziegler (1996). Lifetime imaging of luminescent oxygen sensors based on all-solid-state technology. *Anal. Chem.* **68**, 4512–4514.

39. P. Hartmann, W. Ziegler, G. Holst, and D.W. Lübbers (1997). Oxygen flux fluorescence lifetime imaging. *Sens. Actuat. B* **38**, 110–115.